

Highly localized clustering states in a granular gas driven by a vibrating wall

Eli Livne ¹, Baruch Meerson ¹ and Pavel V. Sasorov ²

¹ Racah Institute of Physics, Hebrew University of Jerusalem, Jerusalem 91904, Israel

² Institute of Theoretical and Experimental Physics, Moscow 117259, Russia

An ensemble of inelastically colliding grains driven by a vibrating wall in two dimensions exhibits density clustering. Working in the limit of nearly elastic collisions and employing granular hydrodynamics, we predict, by a marginal stability analysis, a spontaneous symmetry breaking of the extended clustering state (CS). Two-dimensional steady-state solutions found numerically describe localized CSs with different symmetries. A time-dependent granular hydrodynamic simulation shows that highly localized CSs can develop from natural initial conditions.

PACS numbers: 81.05.Rm, 45.70.Qj, 47.50.+d

Granular flows exhibit fascinating non-equilibrium phenomena and continue to attract much interest [1,2]. We will concentrate here on the striking tendency of granular “gases” (rapid granular flows) to form dense clusters [3]. Clustering results from energy losses by inelastic collisions, and it is a manifestation of thermal condensation instability [4]. Since the discovery of the clustering instability, the validity of granular hydrodynamics [5] has been under scrutiny. In a freely cooling granular gas, all grains eventually come to rest, making the hydrodynamic (and even kinetic) description problematic. A driven granular gas is more convenient for this purpose, as hydrodynamics can be tested on its steady states. The simplest system of this kind is a sub-monolayer of colliding grains in two dimensions, driven by a vibrating wall at zero gravity. This and related two-dimensional systems were investigated by molecular dynamic (MD) simulations [6–8] and in experiment [9]. Experiment in three dimensions (in low gravity) has been also performed [10]. For sufficiently high gas densities, an extended clustering state (CS) was observed away from the driving wall. Comparisons of the steady-state density profiles with those predicted by granular hydrodynamics showed that hydrodynamics is valid only if the grain collisions are nearly elastic [6–8,11].

We demonstrate in this work that this simple system exhibits a surprisingly rich nonlinear behavior already in the limit of nearly elastic collisions. It will be shown that the previously found extended CS can become unstable, and localized CSs of different symmetries appear. These findings put this system in the list of pattern-forming systems out of equilibrium [12].

Let us consider a big ensemble of identical spherical grains of diameter d and mass m_g rolling on a smooth horizontal surface of a rectangular box with dimensions $L_x \times L_y$. The number density of grains is $n(x, y)$. For a sub-monolayer coverage the maximum value of n corresponds to the (hexagonal) close-packing value $n_c = 2/(\sqrt{3}d^2)$. For simplicity, grain collisions with the walls are assumed elastic. The vibrating wall, located at $x = L_x$, supplies energy to the system, see below. This

energy is being lost through inelastic hard-core grain collisions. We neglect the grain rotation and parameterize the inelasticity of grain collisions by a single normal restitution coefficient r . The regime of nearly elastic collisions we will work in corresponds to a strong inequality $1 - r^2 \ll 1$.

Hydrodynamic steady states are described by the equations of momentum and energy balance:

$$p = \text{const}, \quad \nabla \cdot (\kappa \nabla T) = I, \quad (1)$$

where p is the granular pressure, κ is the thermal conductivity, I is the rate of energy losses by collisions and T is the granular temperature (the average kinetic energy per unit mass). To proceed, one needs an equation of state $p = p(n, T)$ and relations for κ and I in terms of n and T . In the low-density limit, $n \ll n_c$, these relations can be derived from the Boltzmann equation (see, e.g. Ref. [13]). The high-density limit, $n_c - n \ll n_c$, was considered by Grossman *et al.* [6]. They also suggested (and verified in MD simulations) convenient interpolations between the low- and high-density limits. We will adopt this practical approach and use their interpolations throughout this paper. In our notation

$$p = m_g n T \frac{n_c + n}{n_c - n}, \quad (2)$$

$\kappa = (\mu/l) m_g n (\alpha l + d)^2 T^{1/2}$ and $I = (\mu/\gamma l) m_g (1 - r^2) n T^{3/2}$. Here l is the mean free path of the grains,

$$l = \frac{1}{\sqrt{8\pi n d}} \frac{n_c - n}{n_c - an}, \quad (3)$$

$a = 1 - (3/8)^{1/2}$, and α and γ are numerical factors of order unity. Grossman *et al.* [6] found that $\alpha \simeq 1.15$ and $\gamma \simeq 2.26$. The value of μ , another numerical factor of order unity, is irrelevant in the steady-state problem, as it cancels out in Eq. (1).

Eq. (1) should be supplemented by boundary conditions. These include the no-flux conditions $\nabla_n T = 0$ at the immobile walls $x = 0$, $y = 0$ and $y = L_y$. Previously, a constant granular temperature was prescribed at the

“thermal wall” $x = L_x$ (in our notation) [6–8,14]. We will use a different boundary condition which simulates the vibrating wall more directly. Our main results, however, will hold for the thermal wall as well.

The problem of computing the energy flux q from a vibrating wall into a granular medium has been addressed in several works [15]. Let the wall velocity oscillate sinusoidally with the amplitude v_m . We assume that v_m is much less than the average grain velocity near the wall, $T_w^{1/2}$. This limit (but with a non-zero gravity) was considered by Kumaran [16]. A direct calculation analogous to his yields $q = (2/\pi)^{1/2} v_m^2 p T^{-1/2}$ [17]. In the language of hydrodynamics, q is the heat flux at the wall:

$$\kappa \partial T / \partial x = (2/\pi)^{1/2} v_m^2 p T^{-1/2} \text{ at } x = L_x. \quad (4)$$

Finally, there is normalization condition:

$$\int_0^{L_x} \int_0^{L_y} n(x, y) dx dy = \langle n \rangle L_x L_y, \quad (5)$$

where $\langle n \rangle$ is the average grain density.

Using Eq. (2), we eliminate T in favor of n and p . In its turn, p can be eliminated by integrating Eq. (1) over the whole box and using the Gauss theorem and Eq. (4). It is convenient to write the governing equations in a scaled form. Introduce scaled coordinates: $\mathbf{r}/L_x \rightarrow \mathbf{r}$ so that the box dimensions become $1 \times \Delta$, where $\Delta = L_y/L_x$ is the aspect ratio of the box. Introducing the (scaled) inverse granular density $z(x, y) = n_c/n(x, y)$, we obtain

$$\nabla \cdot (F(z) \nabla z) = \mathcal{L} Q(z). \quad (6)$$

The boundary conditions are

$$\nabla_n z = 0 \text{ at } x = 0, y = 0 \text{ and } y = \Delta, \quad (7)$$

and

$$\left(G(z) \frac{\partial z}{\partial x} \right) \Big|_{x=1} = \mathcal{L} \frac{\int_0^1 \int_0^\Delta Q dx dy}{\int_0^\Delta H[z(1, y)] dy}. \quad (8)$$

The normalization condition (5) becomes

$$\int_0^1 \int_0^\Delta z^{-1} dx dy = f \Delta, \quad (9)$$

while functions F, G, H and Q are the following:

$$F(z) = \frac{(z^2 + 2z - 1)[\alpha z(z-1) + \sqrt{32/3}(z-a)]^2}{(z-a)(z-1)^{1/2} z^{3/2} (z+1)^{5/2}}, \quad (10)$$

$$G(z) = \frac{(z^2 + 2z - 1)[\alpha z(z-1) + \sqrt{32/3}(z-a)]^2}{z(z-a)(z-1)(z+1)^2}, \quad (11)$$

$$H(z) = \frac{F(z)}{G(z)} \text{ and } Q(z) = \frac{(z-a)(z-1)^{1/2}}{(z+1)^{3/2} z^{1/2}}. \quad (12)$$

Finally, $\mathcal{L} = (32/3\gamma)(L_x/d)^2(1-r^2)$. The other two governing parameters are the grain area fraction $f = \langle n \rangle/n_c$ and Δ .

Eqs. (6)-(9) make a closed set. Their one-dimensional solution $z = Z(x)$ is described by equations

$$(FZ')' = \mathcal{L} Q, \quad Z'|_{x=0} = 0 \text{ and } \int_0^1 Z^{-1} dx = f, \quad (13)$$

where primes stand for the x -derivatives. Notice that Eq. (8) is now satisfied automatically. Eqs. (13) coincide with those obtained by Grossman *et al.* [6] for a thermal wall at $x = 1$ [18]. Eqs. (13) can be solved analytically in the high- and low-density limits [6]. Most interesting, however, is the intermediate regime with a dense cluster (extended CS) located close to $x = 0$, and a low-density region elsewhere. In this case Eqs. (13) should be solved numerically. Examples are presented in Ref. [6], and a similar CS was observed experimentally [9]. We will show now that the extended CS can give way, via a spontaneous symmetry breaking, to highly localized CSs. First, a marginal stability (MS) analysis will show loss of stability of the extended CS. Then, solving Eqs. (6)-(9) numerically, we will find localized CSs with different symmetries. Finally, a time-dependent granular hydrodynamic simulation will show that highly localized CSs can develop from natural initial conditions.

Linearizing Eqs. (6)-(9) around the extended CS $z = Z(x)$ and looking for a small correction in the form of $\psi(x) \cos(\pi my/\Delta)$, where $m = 1, 2, \dots$, we obtain

$$F\phi'' - (\mathcal{L} Q_Z + \pi^2 m^2 \Delta^{-2} F) \phi = 0, \quad (14)$$

where $\phi = F\psi$ and index Z means the z -derivative evaluated at $z = Z(x)$. The boundary conditions are

$$\phi'|_{x=0} = 0, \quad (FG\phi' + Z'(FG_Z - GF_Z)\phi)|_{x=1} = 0. \quad (15)$$

Functions F and G which enter Eqs. (14) and (15) are evaluated at $z = Z(x)$.

For fixed values of parameters \mathcal{L} , f and m , Eqs. (14) and (15) represent an eigenvalue problem for the aspect ratio $\Delta = \Delta_m(\mathcal{L}, f) = m \Delta_1(\mathcal{L}, f)$. The extended CS loses stability when $\Delta > \Delta_m$. For the fundamental mode $m = 1$ (or $\lambda/2$, one half of the wavelength across the system in the y -direction) this critical value Δ_1 is the lowest. Figure 1 shows, for different values of \mathcal{L} , the MS curves $\Delta = \Delta_1(f)$ found by solving Eqs. (13) - (15) numerically. Above the MS curves localized CSs must develop. Interestingly, the extended CS remains linearly stable *for any* Δ beyond a finite interval of the area fractions $f_1(\mathcal{L}) < f < f_2(\mathcal{L})$ such that $f_1 > 0$ and $f_2 < 1$. As \mathcal{L} increases, the instability interval (f_1, f_2) shrinks, while

the minimum value of Δ_1 decreases: $\Delta_1^{(min)} \simeq 140 \mathcal{L}^{-1/2}$ [19]. For sufficiently large \mathcal{L} , $\Delta_1^{(min)}$ becomes less than 1. See Fig. 2 which shows the instability tongues $m = 1$ and $m = 2$ for $\mathcal{L} = 5 \cdot 10^4$.

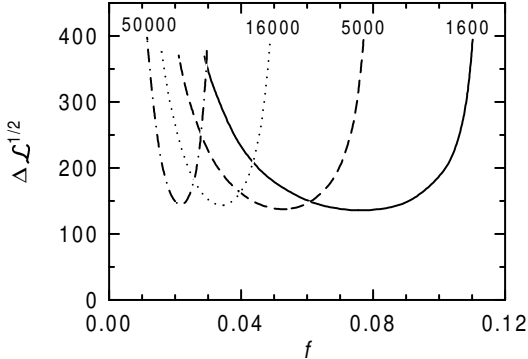


FIG. 1. Marginal stability curves $\Delta_1(f)$ for different values of \mathcal{L} . The values of Δ_1 are multiplied by $\mathcal{L}^{1/2}$.

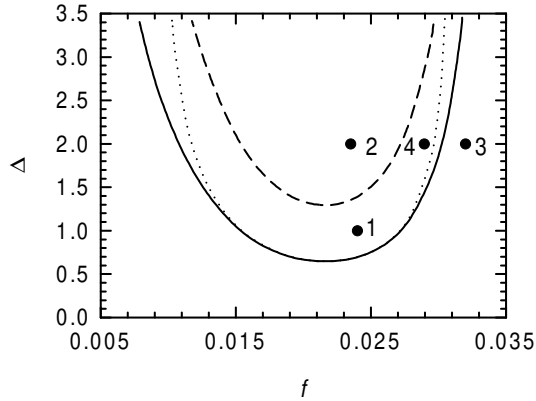


FIG. 2. Marginal stability (MS) curves $\Delta_m(f)$ for $m = 1$ (solid line) and 2 (dashed line) and $\mathcal{L} = 5 \cdot 10^4$. Density profiles corresponding to points 1,2,3 and 4 are shown in Fig. 3. The dotted line shows the MS curve $m = 1$ for the “thermal wall”.

When $f \ll \min(1, \mathcal{L}^{-1/2})$ the asymptotics of $\Delta_1(f)$ can be found analytically. In this case the whole system is in the dilute limit, $z \gg 1$ (still, it is necessary to account for the subleading terms). In addition, $Z(1) - Z(0) \ll 1$ in this case, so Taylor expansion of $Z(x)$ and $\psi(x)$ up to x^4 suffice. After some algebra, Eqs. (13) - (15) yield

$$\Delta_1 = \pi \left(\frac{\mathcal{L}^2 f^4}{3\alpha^4} - \frac{(1+a)\mathcal{L} f^3}{\alpha^2} \right)^{-1/2}. \quad (16)$$

It follows from Eq. (16) that $f_1(\mathcal{L}) = 3\alpha^2(1+a)\mathcal{L}^{-1}$.

The extended CS can be also unstable when the wall $x = L_x$ is a “thermal wall”. Solving the corresponding eigenvalue problem [where the second boundary condition in Eq. (15) is replaced by $\phi(x = 1) = 0$], we obtained instability tongues similar to those for the vibrating wall, but more narrow. Figure 2 shows the instability tongue

$m = 1$ for $\mathcal{L} = 5 \cdot 10^4$. Noticeable is the coincidence of the $m = 1$ curves at intermediate f for the two types of driving walls. It results from a strong localization of the eigenfunction $\phi(x)$ near the wall $x = 0$ at large \mathcal{L} . The exact form of the boundary condition at $x = 1$ is not important in this regime. Finally, for the thermal wall the localized CS is stable for any Δ if $f \ll \min(1, \mathcal{L}^{-1/2})$, in contrast to the vibrating wall.

In the rest of the paper we will deal with the vibrating wall. Within the instability tongues of Fig. 1 the MS analysis is invalid. Besides, it can miss a subcritical bifurcation outside of the instability tongues. Therefore, we solved the two-dimensional steady-state equations (6)-(9) numerically (a nonlinear Poisson solver, Newton’s iterations), exploring some parts of the parameter plane (f, Δ) of Fig. 2. Figure 3 shows the density profiles of 4 typical steady states. Highly localized nonlinear $\lambda/2$ - and λ -states are evident in Fig. 3a and b. They are not unexpected, as points 1 and 2 lie inside the instability tongue $m = 1$ and $m = 2$, respectively. In general, we found that when crossing the MS curve $\Delta = \Delta_1(f)$ from the left (along the line $\Delta = 2$), or from below, one goes continuously from an extended CS to a “weakly two-dimensional” $\lambda/2$ -state. This implies a supercritical bifurcation. However, when moving from the right to the left along the line $\Delta = 2$, nonlinear $\lambda/2$ - and λ -states appear *inside* the linear stability regions of the extended CS and of the mode $m = 1$, respectively, and *coexist* with the extended CS (with the mode $m = 1$, respectively). These findings give evidence for bistability and subcritical bifurcations. Examples of subcritical $\lambda/2$ - and λ -states are shown in Fig. 3c and d.

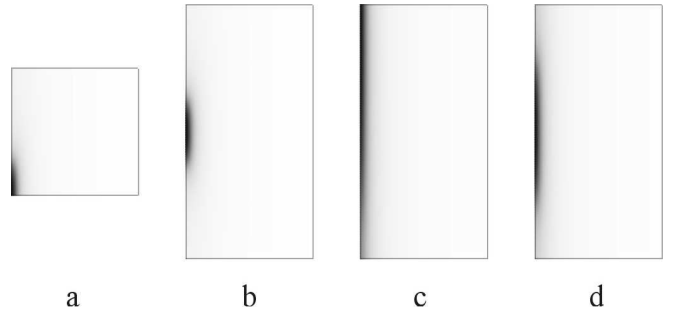


FIG. 3. Steady-state density profiles (gray scale, separate for each picture) corresponding to points 1 (a), 2 (b), 3 (c) and 4 (d) of Fig. 2. The maximum (minimum) density at the wall $x = 0$ is 0.76 (0.036) (a and b), 0.48 (0.21) (c) and 0.54 (0.10) (d). The gas density at the vibrating wall $x = 1$ is close to $4 \cdot 10^{-3}$ for all profiles.

Are localized CSs stable, and can they be reached from natural initial conditions? To answer these questions, we performed *time-dependent* hydrodynamic simulations. We will briefly report here a single simulation (a detailed account will be given elsewhere). The full hydrodynamic equations were solved with the same constitutive rela-

tions and boundary conditions as in our steady-state analysis. Instead of the shear viscosity, we accounted for a rolling friction force $-nv/\tau$. An extended version of the code VULCAN [20] was used. The code employs flexible moving grids and can operate in any combination of Eulerian and Lagrangian modes. We used the Van Leer scheme [21], which preserves second order accuracy, in the rezoning stage. The initial scaled density in this example was $n(x, y, t = 0) = f + 0.1 f \cos(2\pi y/\Delta)$ (independent of x). Figure 4 shows the density evolution. One can see that a CS develops away from the driving wall. With time, the CS becomes more and more localized in the y -direction and approaches the steady-state profile shown in Fig. 3b.

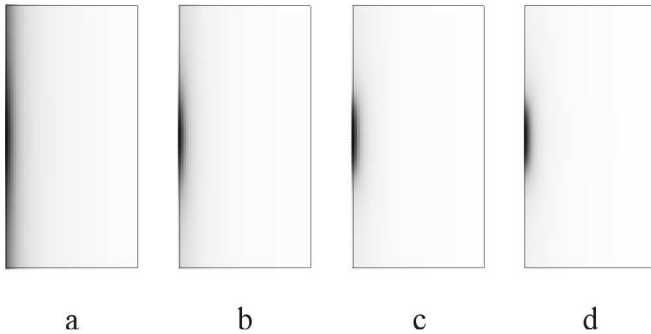


FIG. 4. Density evolution for $\mathcal{L} = 5 \cdot 10^4$, $\Delta = 2$ and $f = 0.0235$. Shown are the density profiles (gray scale, separate for each picture) at scaled times 100 (a), 500 (b), 1,000 (c) and 1,290(d). The maximum (minimum) density at the wall $x = 0$ is 0.25 (0.14) (a), 0.46 (0.072) (b), 0.66 (0.040) (c) and 0.74 (0.036) (d). The gas density at the vibrating wall $x = 1$ is close to $4 \cdot 10^{-3}$ for all profiles.

In summary, we predict a spontaneous transition from the extended to highly localized CSs in a granular gas driven by a vibrating wall. This prediction poses new questions, and first of all about the character of bifurcations and pattern selection and coarsening. A better understanding of this simple system will help to understand more complicated regimes of rapid granular flows, such as the recently observed thermal convection [22]. The second group of questions concerns the role of fluctuations, the normal stress difference and other non-hydrodynamic effects observed at finite $1 - r^2$ [7,8]. Therefore, it would be very interesting to investigate the localized CSs in MD simulations and in experiment. The aspect ratios used in Refs. [6,7,9] were lower than the corresponding values of $\Delta_1^{(min)}$ which explains stability of the extended CSs observed in these works. MD simulations and experiments performed inside an instability tongue of Fig. 1 are expected to produce localized CSs.

We acknowledge a useful discussion with E. Ben-Naim and J. Fineberg. This research was supported by the Israel Science Foundation founded by the Israel Academy of Sciences and Humanities, and by the Russian Founda-

tion for Basic Research (grant No. 99-01-00123).

- [1] H.M. Jaeger, S.R. Nagel, and R.P. Behringer, Rev. Mod. Phys. **68**, 1259 (1996); Physics Today, April 1996, p. 32.
- [2] L.P. Kadanoff, Rev. Mod. Phys. **71**, 435 (1999).
- [3] M.A. Hopkins and M.Y. Louge, Phys. Fluids A **3**, 47 (1991); I. Goldhirsch and G. Zanetti, Phys. Rev. Lett. **70**, 1619 (1993); S. McNamara and W.R. Young, Phys. Rev. E **53**, 5089 (1996).
- [4] Similar thermal condensation instabilities develop in radiatively cooling plasmas; for a review see B. Meerson, Rev. Mod. Phys. **68**, 215 (1996).
- [5] P.K. Haff, J. Fluid Mech. **134**, 401 (1983); C.S. Campbell, Annu. Rev. Fluid Mech. **22**, 57 (1990).
- [6] E.L. Grossman, T. Zhou, and E. Ben-Naim, Phys. Rev. E **55**, 4200 (1997).
- [7] J.J. Brey and D. Cubero, Phys. Rev. E **57**, 2019 (1998).
- [8] S.E. Esipov and T. Pöschel, J. Stat. Phys. **86** 1385 (1997).
- [9] A. Kudrolli, W. Wolpert, and J.P. Gollub, Phys. Rev. Letters **78**, 1383 (1997).
- [10] É. Falcon *et al.*, Phys. Rev. Lett. **83**, 440 (1999).
- [11] Hydrodynamics is expected to be valid when the mean free path of the grains is much smaller than any length scale (and the mean collision time is much smaller than any time scale) described hydrodynamically. These conditions are easy to satisfy for nearly elastic collisions.
- [12] M.C. Cross and P.C. Hohenberg, Rev. Mod. Phys. **65**, 851 (1993).
- [13] J.J. Brey, J.W. Dufty, C.S. Kim, and A. Santos, Phys. Rev. E **58**, 4638 (1999).
- [14] Ref. [7] actually used constant (and equal) temperatures at two opposite walls.
- [15] S. McNamara and S. Luding, Phys. Rev. E **58**, 813 (1998); and references therein.
- [16] V. Kumaran, Phys. Rev. E **57**, 5660 (1998).
- [17] In the opposite limit $T_w^{1/2} \ll v_m$ we found $q = 2\pi v_m p$. Interpolating between these two limits, we obtain a practical relation $q = 2\pi v_m p (1 + 2^{1/2} \pi^{3/2} \epsilon)^{-1}$ which should work well for any $\epsilon = T_w^{1/2} / v_m$.
- [18] The one-dimensional density profile is the same for the two types of walls. The equilibrium pressure is different, leading to a difference, by a constant factor, in the temperature profile.
- [19] It corresponds to $L_y^{(min)} \simeq 43 \gamma^{1/2} d (1 - r^2)^{-1/2}$ in the “physical” variables.
- [20] E. Livne, Astrophys. J. **412**, 634 (1993).
- [21] B. Van Leer, J. Comput. Phys. **32**, 101 (1979).
- [22] R. Ramírez, D. Rissó, and P. Cordero, Phys. Rev. Lett. **85**, 1230 (2000).